Nanoscale Advances

ROYAL SOCIETY OF CHEMISTRY

PAPER

View Article Online
View Journal | View Issue

Cite this: *Nanoscale Adv.*, 2020, **2**, 1290

Understanding the driving forces of camptothecin interactions on the surface of nanocomposites based on graphene oxide decorated with silica nanoparticles

Leandro C. Fonseca, * Marcelo de Sousa, Djalma L. S. Maia, Luis Visani de Luna and Oswaldo L. Alves*

Camptothecin (CPT) is a potent antitumor drug frequently used in studies of drug delivery systems. The poor water solubility and unfavourable pharmacokinetic conditions of CPT and the development of nanomaterials such as mesoporous silica nanoparticles (MSNs), graphene oxide (GO) and a new family of GO decorated with MSNs (GO-MSNs) motivated the present work, which sought to solve these challenges. In this context, release assays showed rapid and prolonged release, respectively, by silica and GO/GO-MSN nanomaterials; release was faster at pH 7.4 and slower at pH 5.0 in all situations. In particular, GO-MSNs presented an important advantage compared to GO due to their slower drug release at pH 7.4 (physiological conditions in blood; slowest release is expected under these conditions) and faster drug delivery at pH 5.0 (acidic conditions in endosomes of cancer cells; fastest release is expected under these conditions). The results, therefore, present the GO-MSN nanomaterial as a potential candidate for antitumor applications. The main drug–nanocarrier chemical interactions (London forces, hydrogen bonds, and electrostatic and dipole–dipole interactions) are also exhaustively described in order to understand the observed differences in drug delivery properties among these nanomaterials and to comprehend the influence of pH on concomitant and dynamic interactions.

Received 29th November 2019
Accepted 5th February 2020

DOI: 10.1039/c9na00752k

rsc.li/nanoscale-advances

1. Introduction

Chemotherapy is the most common type of antitumor treatment and consists of the application of antitumor drugs in the fight against cancer cells.[1,2] In this context, some of the current challenges in the use of these biological drugs, especially hydrophobic species, include the following:

- Their low solubility in blood, a hydrophilic fluid, resulting in an insufficient uptake by tumour cells[3–5] and requiring an increased applied dose concentration;

- Loss of biological activity shortly after intravenous administration, such as that observed for drugs that are inactive under the physiological conditions found in blood,[6] also requiring doses at increased concentrations;

- The biodegradability of the free drug during application, also leading to a loss of biological activity;[6]

- Deficient biodistribution in the body, causing the applied free drug to reach not only tissues affected by tumours but also healthy tissues, leading to serious side effects;[6]

- Unfavourable pharmacokinetic conditions, *i.e.*, the applied drug is rapidly eliminated from the body by the kidneys, requiring an increased dose concentration or continuous application.[6]

Some hydrophobic antitumor drugs such as curcumin (Cur)[7] and camptothecin (CPT),[8] among others, present challenges such as those mentioned above, which motivated our group to choose one of them, camptothecin (as a model drug), to solve some of these problems. CPT is a substance that was discovered in 1966, is extracted naturally from the herb *Camptotheca acuminata*[9] and has been reported as a potent antitumor drug that plays an important role in the inhibition of DNA topoisomerase I (TOPO I).[10] More specifically, TOPO I acts during DNA relaxation prior to replication, transcription and translation by cleaving one of the DNA strands, restoring the bonds and repeating the cycle, which is essential for cell multiplication and maintenance.[11] In this context, camptothecin interacts with TOPO I, preventing the restoration of bonds in DNA and consequently inducing cell death by apoptosis. CPT is also an FDA-approved drug-like molecule, similar to species such as topotecan, irinotecan[9] and other substances under preclinical phase studies of lurtotecan and silatecan.[12] CPT is a molecule comprising organic functions such as lactam, conjugated aromatic rings, hydroxyl and lactone (lac) groups (Fig. 1).[13] The

Laboratory of Solid State Chemistry, Institute of Chemistry, Universidade Estadual de Campinas, 13083-970, Campinas, São Paulo, Brazil. E-mail: leandro.fonseca89@gmail.com; oalves@iqm.unicamp.br

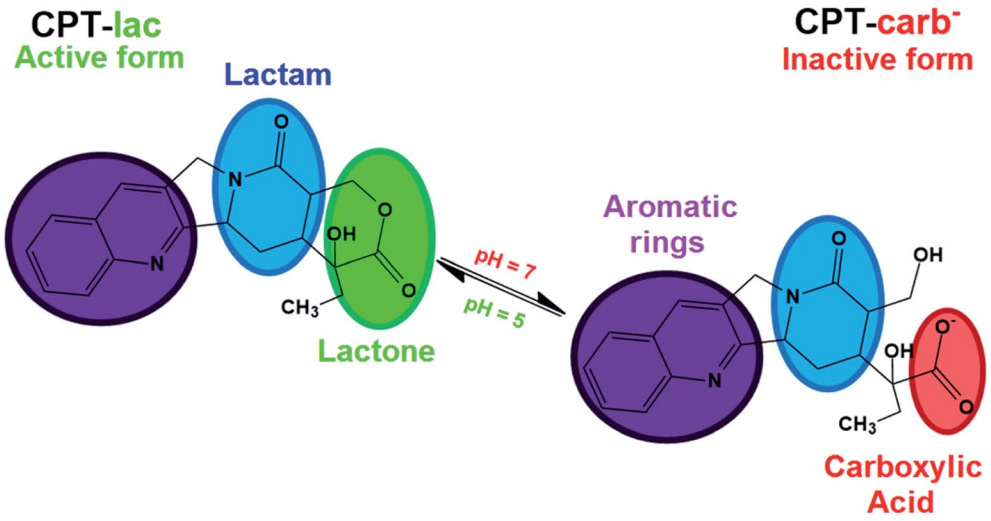

Fig. 1 Molecular structure of camptothecin (CPT) in its two lactone (CPT-lac) and carboxylate (CPT-carb$^-$) forms in pH dependent chemical equilibrium.

organic lac function maintains the biological activity of this drug at pH 5.0, which is typical of cancer cell endosomes. At neutral pH (physiological conditions in organisms), the lactone function is hydrolysed to form the carboxylate (carb$^-$) function, resulting in antitumor inactivity.[14–17] pH significantly regulates the biological activity of this drug in the active lactone form (CPT-lac) in chemical equilibrium with the inactive carboxylate form (CPT-lac$^-$). Significant efforts are currently directed at the development of nanocarriers to solve the problems of low drug solubility in blood and under unfavourable pharmacokinetic conditions (rapid release), as in the case of CPT. In this context, nanomaterials can effectively transport these molecules to cancer cells, facilitating their delivery and intracellular uptake,[18] prolonging their release time and optimizing their distribution in the body. In addition, these molecular carriers can be developed as high-capacity platforms for encapsulating antitumor drugs,[19–21] an important property for optimizing the amount of antitumor drugs within the cells. The main nanocarriers include graphene oxide (GO),[22–24] mesoporous silica nanoparticles (MSNs)[25–27] and a new family of nanocomposites based on graphene oxide decorated with silica nanoparticles (GO-MSNs).[28,29]

Graphene oxide is a two-dimensional carbon nanomaterial comprising regions of carbon atoms with sp^2 hybridization and sp^3 carbons associated with oxygenated functional groups, including carboxylic acid, ketone, aldehyde, epoxide, hydroxyl and lactol groups.[30] This material intrinsically has interesting characteristics, such as good water dispersibility, high mechanical strength and a significant theoretical surface area (2630 $m^2\ g^{-1}$).[30] These important properties of GO contribute to its wide range of possible applications in photocatalysis,[31] supercapacitors[32] and biosensors.[33] However, the use of GO in antitumor applications is still a new scientific trend. Studies related to GO materials comprising CPT as a drug host molecule are still rare and show promising results from the point of view of high encapsulation capacity.[34,35] However, the literature has reported toxic effects of GO, such as cell membrane damage and a high capacity to cause haemolysis,[30,36] thus increasing the chance of toxicity in intravenous applications. There are also studies that show opposite effects, characterized by a low haemolytic effect. The controversial biological results may be related to the employed method of production of these materials. The surface functionalization of this nanomaterial with polymers has been shown to be strategic from the point of view of biocompatibility and nanosafety. Because research in this direction is still new, the influence of the external environment on the physicochemical interactions of graphene oxide with hydrophobic antitumor drugs such as CPT is not very well understood. In this context, understanding the influence of biological conditions such as pH on nanomaterial–molecule interactions is one of the objectives of the present work.

Mesoporous silica nanoparticles are nanomaterials with important physicochemical characteristics, including the presence of surface silanol groups (Si–OH) that allow several functionalization strategies for the acquisition of new properties. The high surface area (>900 m^2 g) and presence of pores in these nanoparticles allow the encapsulation of desired molecules.[30] In this context, the interior of the nanoparticles can be functionalized with hydrophobic organic groups to enable further interaction with antitumor drugs (which are mostly hydrophobic), and the outer surface can be chemically modified to optimize colloidal stability[7] and biocompatibility[27] and for covalent attachment in nanomaterials such as graphene oxide. Studies related to the use of MSNs in CPT encapsulation processes are better known and include important studies showing distinct incorporation strategies, purification methods, long-term drug release tests and *in vitro*/*in vivo* applications.[25–27] The mentioned studies use drug encapsulation strategies through non-covalent chemical interactions. In such cases, the strength of drug–pore interactions is dependent on the presence of functionalized organic functions on the inner surface of silica nanoparticles. The presence of these

hydrophobic species is crucial for minimizing premature drug release during systemic circulation and for optimizing the retention of the host molecule. Recent studies have shown new strategies of CPT incorporation into silica nanoparticles through covalent bonds[37–39] that optimize interactions with the nanostructure. Despite efforts in the development of mesoporous silica nanoparticles encapsulated with CPT, these nanomaterials present a low encapsulation capacity limited to 20%, and the majority of the results are in the range of 1 to 9%.[25,27] In this context, understanding drug–nanocarrier chemical interactions based on encapsulation optimization is another focus of the present work.

A new family of nanocomposites based on graphene oxide decorated with spherical mesoporous silica nanoparticles has recently been reported,[40,41] and interesting results have been obtained from the point of view of their application as nanocarriers. Huang *et al.*[40] obtained a nanocomposite of GO functionalized with silica nanoparticles containing smaller nanoparticles of iron oxide and quantum dots of ZnO in its pores and proved its application as a magnetic nanocarrier and for bioimaging. Yang *et al.*[41] reported the development of a graphene oxide nanocomposite decorated with silica nanoparticles containing a magnetic core of Fe_3O_4 nanoparticles and externally functionalized with polyethyleneimine (PEI), used for the encapsulation of gambogic acid (GA), an antitumor molecule. As a new trend in nanocarrier applications, GO-MSNs are novel nanomaterials from the point of view of interactions with biological systems, such as haemolytic and protein interactions (corona effect), and can be used to investigate the body's biological responses (including the immune system). The evaluation of haemolytic and corona effects by GO-MSNs was first performed in our previous work,[30] which showed reduced levels of haemolysis and minimization of protein adsorption; the results indicated that these nanocomposites are possible biocompatible materials.

Therefore, the motivation of the present work is the comparative encapsulation of camptothecin in nanocomposites of graphene oxide decorated with silica nanoparticles as well as in the raw nanomaterials, MSNs and GO. The drug–nanocarrier chemical interactions were individually assessed, discussed and compared in all situations to understand the differences in the encapsulation capacity and drug release properties over time of each nanomaterial. Especially for the nanocomposite, first developed by our group, the CPT–(GO-MSN) interaction is discussed for the first time. In this context, the amount of adsorbed drug on each of these nanomaterials was comparatively quantified in order to assess the efficiency of three types of drug delivery systems. In addition, drug release studies of GO-MSN and their comparison with CPT release properties of the raw nanomaterials (GO and MSN) were also performed for the first time and reveal release phenomena and interactions fully discussed from fundamental chemistry concepts.

2. Experimental

2.1. Materials

Camptothecin (CPT, >90.0%) was obtained from Oakwood Chemical (USA). Dialysis membranes (MWCO: 3.5 kDa) were obtained from Spectra/Por (USA). Tablets of phosphate buffer were obtained from Sigma Aldrich (USA). A polysorbate 80 surfactant (Tween 80-T80) was obtained from Makeni Chemicals (Brazil). Mesoporous silica nanoparticles with internal phenyl groups and external amino functions (MSNs), graphene oxide (GO) and nanocomposites based on graphene oxide decorated with 10 wt% added MSNs (GO-MSN_{10}) were obtained as described in our previous work.[30] The characterization data of these nanomaterials are also available in our previously published work.[30]

2.2. CPT encapsulation in MSN, GO and GO-MSN_{10} nanomaterials

Camptothecin encapsulation was performed in mesoporous silica nanoparticles (MSNs), graphene oxide (GO) and nanocomposites based on graphene oxide decorated with mesoporous silica nanoparticles (GO-MSN_{10}).

Camptothecin encapsulation in MSNs was performed according to the described protocol in the work published by de Paula *et al.*,[27] with some modifications. In this context, 10 mg of nanoparticles suspended in 20 mL of deionized water (0.5 mg mL^{-1}) was sonicated for 10 minutes, followed by the addition of 10 mg of camptothecin (the MSN : CPT mass ratio was 1 : 1). The system was sonicated again for 10 minutes and subjected to constant stirring for 12 h in the absence of light and at room temperature. Purification of the silica nanoparticles containing encapsulated camptothecin was performed by two cycles of centrifugation at 500 rpm for 2 minutes at room temperature. In this process, the bottom solid was the excess free camptothecin, and the supernatant was the product of interest. The latter was subjected to a decanting process for 48 h to optimize the purification process. In this last stage, therefore, the supernatant containing the target nanomaterial was separated from the free decanted CPT and stored as dispersion at a concentration of 0.5 mg mL^{-1} at 4 °C. The encapsulation capacity (EC) of camptothecin in the sample was determined according to the quantification procedure described below. The obtained sample was denoted as MSN + CPT.

Camptothecin encapsulation in GO was performed according to a described protocol in the published work of de Sousa *et al.*[34] In this process, a solution of 10 mg CPT in 2 mL of dimethyl sulfoxide (DMSO) was prepared. Subsequently, this solution was added dropwise to a dispersion of 10 mg of graphene oxide in 18 mL of deionized water under constant stirring. The formed mixture was sonicated for 10 minutes and subsequently kept under constant stirring for 12 h in the absence of light and at room temperature. The purification of graphene oxide-encapsulated camptothecin was accomplished by filtration with a 0.22 μm PVDF membrane, followed by washing three times with 20 mL of a 1 : 1 (v : v) water- : methanol mixture and twice with 20 mL of water to eliminate excess free camptothecin. In this process, after each filtration, the resulting solid on the membrane was suspended in the wash fluid by sonication for 5 minutes, after which filtration and subsequent washing were repeated. At the end of the last wash, the final product was suspended in 20 mL of deionized

water (0.5 mg mL^{-1} of GO) and stored at 4 °C. The sample was denoted as GO + CPT.

Camptothecin encapsulation in GO-MSN_{10} was performed using the above method by only changing the volume of DMSO (4 mL) in the preparation of the drug solution and the volume of water (36 mL) in the initial dispersion of GO-MSN_{10}; the other process variables remained the same, and the production steps were executed in a similar manner to the above method. The resulting dispersion was stored at 4 °C at a GO-MSN_{10} concentration of 0.5 mg mL^{-1}. The sample was denoted as GO-MSN_{10} + CPT. The EC values of camptothecin in the GO + CPT and GO-MSN_{10} + CPT dispersions were determined according to the quantification procedure described below.

For CPT quantification in the MSN + CPT, GO + CPT and GO-MSN_{10} + CPT samples, 100 μL of each dispersion was added to 4.9 mL of methanol. The formed system was subjected to 30 minutes of sonication and centrifuged at 15 000 rpm at 4 °C for 30 minutes. Thus, CPT (soluble in methanol) was extracted from the nanomaterial, and the latter was obtained as a decanted solid in the centrifuge tube. A volume of 1 mL of the supernatant (consisting of free extracted camptothecin) was subjected to UV-Vis analysis to obtain the absorbance at 360 nm; the resulting value was compared to the calibration curve for the encapsulated drug. The quantification procedure was performed in triplicate.

2.3. CPT release studies from the MSN + CPT, GO + CPT and GO-MSN_{10} + CPT materials

Drug release assays of the MSN + CPT, GO + CPT and GO-MSN_{10} + CPT nanomaterials were performed by adding 3 mL of each dispersion to a dialysis membrane (MWCO: 3.5 kDa). The membrane containing the nanomaterial was immersed in two types of release media: 100 mL of phosphate buffer (pH 7.4), mimicking the pH of physiological conditions in living organisms, and 100 mL acetate buffer (pH 5.0), mimicking the pH of endosomes, acidic organelles found in cancer cells. Both media contained 1% (v/v) Tween 80, a neutral surfactant used to facilitate camptothecin release from the nanomaterials, since the hydrophobic nature of this drug also contributes to increased interactions with the nanostructures present in the described hydrophilic fluids. The release studies were performed at 37 °C (human body temperature) for 192 h. In this period, 1 mL of release medium was collected at predetermined time intervals and subjected to UV-Vis absorbance reading at 360 nm. Thus, the released CPT percentage was estimated in relation to the total amount of this drug present in the nanomaterial in the dialysis membrane. For each sample volume collected from the release medium, an equal volume of the corresponding medium was added to maintain a constant volume of 100 mL.

2.4. Characterization of the MSN + CPT, GO + CPT, and GO-MSN_{10} + CPT nanomaterials

The physicochemical characterization of MSN + CPT, GO + CPT, and GO-MSN_{10} + CPT samples was performed using several techniques. Ultraviolet-visible (UV-Vis) absorption spectroscopy was performed on a Shimadzu UV 1650 PC spectrometer. X-ray diffraction (XRD) analyses were performed on a Shimadzu XRD-7000 diffractometer with CuKα X-ray radiation at a wavelength of 1.54056 Å with a voltage generator set to 40 kV ($5° < 2\theta < 50°$) and a scan rate of 2° min^{-1}. The morphology of the nanostructures was observed by transmission electron microscopy (TEM) using a Zeiss LIBRA 120 microscope coupled to an Omega Filter-spectrometer with an accelerating voltage of 80 kV.

3. Results and discussion

3.1. CPT encapsulation in the MSN, GO and GO-MSN_{10} nanomaterials

Mesoporous silica nanoparticles, graphene oxide and the nanocomposite GO-MSN_{10} were subjected to the camptothecin encapsulation process. In this process, the drug was added to the nanomaterial by simple addition and constant stirring at room temperature for 12 h in the absence of light. MSN + CPT, GO + CPT and GO-MSN_{10} + CPT were characterized by UV-Vis, XRD and TEM as previously discussed.

UV-Vis spectra of the nanocarriers in the absence and presence of camptothecin are shown in Fig. 2(A). First, this technique enabled the calculation of the encapsulation capacity of the antitumor drug in each of the nanocarriers: 8.1 ± 0.4% (MSN + CPT), 81.1 ± 3.7% (GO + CPT) and 80.9 ± 0.9% (GO-MSN_{10} + CPT). The GO and GO-MSN_{10} nanocarriers have

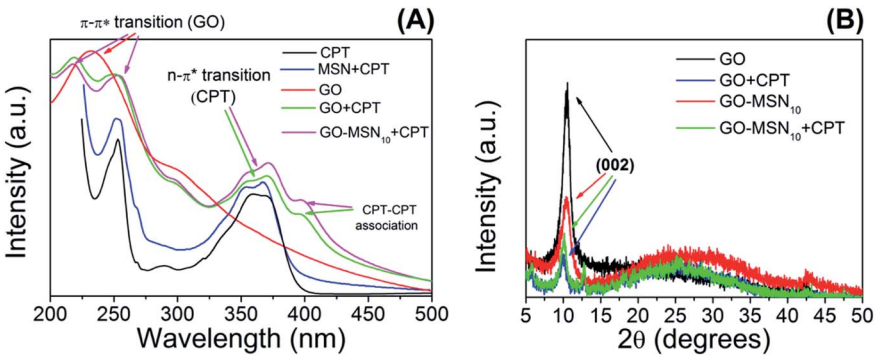

Fig. 2 UV-Vis spectra (A) and XRD patterns (B) of the MSN, GO and GO-MSN_{10} nanomaterials in the absence and presence of camptothecin.

a similar EC. Their percentage values are 10 times higher than those of silica nanoparticles. This result suggests strong drug–nanocarrier interactions for the GO + CPT and GO-MSN_{10} + CPT systems.

The camptothecin spectrum shows a broad band at 365 nm, corresponding to n → π* electronic transitions present in this molecule in its carboxylate (CPT-carb$^-$) form.[13] It is important to mention that the presence of camptothecin mostly in the lactone form (CPT-lac) can be analysed by observing this broad band, but the band contains two shoulders at approximately 355 and 370 nm.[13] As previously discussed, CPT-carb$^-$ and CPT-lac are mostly formed at pH values of approximately 7.4 and 5.0, respectively. From an antitumor action point of view, the carboxylate group-containing structure is inactive against cancer cells, while the structure comprising the lactone ring is biologically active.[17] CPT also has a broad band at 253 nm ascribed to π → π* electronic transitions.[42]

After CPT encapsulation in silica nanoparticles, camptothecin bands at 253 nm (π → π* transitions) and two shoulders at 354 and 368 nm (n → π* electronic transitions) are observed, confirming the presence of CPT in the nanomaterial. The UV-Vis spectrum of graphene oxide (GO) shows a significantly broad band at 232 nm containing a broad shoulder at 294 nm, corresponding respectively to the π → π* electronic transitions of conjugated rings (C═C) and n → π* transitions of C═O groups.[43] The addition of camptothecin to graphene oxide significantly influences the electronic profile of the system, as observed in the GO + CPT spectrum. In this context, two broad bands are observed at 218 and 251 nm, corresponding to overlapping π → π* electronic transitions from GO and CPT. The absence of the intense peak at 232 nm (as previously observed in the GO spectrum) is notable. This set of results suggests physicochemical interactions between graphene oxide and camptothecin by π–π stacking. Fortunately, the spectral region in the wavelength range between 325 and 425 nm comes only from the electronic absorption of camptothecin, making it possible to use this region to draw important conclusions. Unexpectedly, the spectrum of the GO + CPT system presents another band at 396 nm, suggesting a new type of electronic transition not observed in the spectrum of free CPT discussed above. This result has also been observed in previously published studies[22,44,45] related to graphene oxide-based materials containing encapsulated camptothecin. However, these studies do not explain the phenomenon. The hypothesis proposed by our group is that CPT–CPT molecular association is favoured by the presence of graphene oxide as a template, which has a favourable morphology for –GO–**CPT–CPT**– stacking. The high concentration of camptothecin in the GO + CPT sample (81.1 ± 3.7%) is another relevant factor for this intermolecular interaction between camptothecin molecules since an increase in concentration favours this association.[46,47] CPT–CPT interactions have been discussed in the literature[47,48] for other types of nanocarriers and contexts; previous reports corroborate the presented hypothesis, and the current work is the first to discuss such interactions in systems based on graphene oxide.

According to the GO-MSN_{10} + CPT UV-Vis spectrum presented in Fig. 2(A), the electronic effects observed in the CPT encapsulation process are similar to those in the GO + CPT system since the band at 237 nm disappears, while two others are observed at 218 and 251 nm, suggesting π–π stacking between CPT and graphene oxide. The observed bands in the region between 325 and 425 nm have the same profile as those shown in the GO + CPT spectrum, complementing the discussed hypothesis of drug–nanocarrier interactions and suggesting the presence of CPT–CPT interactions on the GO-MSN_{10} surface.

The crystallographic structures of the nanomaterials in the absence and presence of camptothecin were analysed by X-ray diffraction, and the results are presented in Fig. 2(B). The XRD patterns of GO exhibited a diffraction peak for the (002) plane at $2\theta = 10.4°$, indicating an interplanar spacing of 0.84 nm resulting from the introduction of oxygen groups onto the GO surface. The presence of this diffraction peak suggests, in itself, some or few stacked sheets of GO. After the functionalization of GO with MSNs, a decreased intensity in the diffraction peak for the (002) plane was observed, suggesting a decrease in long-range order in the sheets of GO-MSN_{10} due to the decrease in π–π re-stacking. In this context, the addition of silica nanoparticles to the surface of graphene oxide promotes exfoliation, and no intercalation phenomenon was observed since the interplanar spacing, estimated to be $d = 0.84$ nm ($2\theta = 10.4°$), remained constant before and after functionalization with MSNs. The addition of CPT to GO and GO-MSN_{10} also caused a decrease in the peak intensity of the (002) plane in both situations due to a similar effect occurring during the introduction of silica nanoparticles into graphene oxide. In this context, the presence of the drug also reduces the re-stacking of the sheets, improving the exfoliation process and thus increasing chemical accessibility. Additionally, the interplanar spacing of the (002) plane in both samples was estimated at $d = 0.88$ nm ($2\theta = 10.0°$). This result indicates that CPT does not intercalate in these nanomaterials and promotes their exfoliation. This exfoliation phenomenon (reduced π–π stacking) is schematically presented in Fig. 3. The scheme shows the consequences of CPT addition and MSN functionalization in the structures of the corresponding nanocarriers.

Fig. 4(A–C) show transmission electron microscopy (TEM) images of the MSN, GO and GO-MSN_{10} nanomaterials in the presence of camptothecin. The nanoparticles (Fig. 4(A)) maintained a spherical morphology with a porous structure and irregular topography after the addition of camptothecin, retaining the morphological and structural aspects of the used raw material (MSN) described in our previous work.[30] CPT could not be visualized, possibly due to its reduced amount (8.1 ± 0.4%) in the nanoparticles and because it was located in the porous interior. Fig. 4(B) shows the GO + CPT system: the graphene oxide sheets are indicated by red arrows, and the unexpected formation of camptothecin crystals is indicated by blue arrows. The image reveals GO sheets with micrometric dimensions that retain the structural integrity of the used raw material (GO) described in our previous work.[30] In addition, the CPT crystals reveal a needle-like morphology with micrometric lengths. The formation of this chemical structure corroborates the discussed hypothesis regarding CPT–CPT interactions on

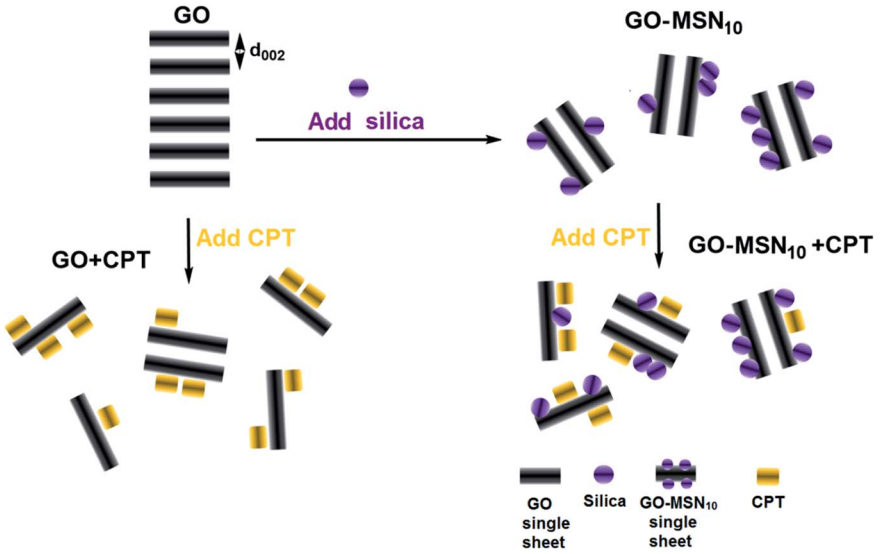

Fig. 3 Structural effects resulting from CPT addition (CPT) and functionalization of MSNs in GO and GO-MSN$_{10}$; d_{002} is the interplanar spacing of the 002 planes.

the surface of GO and GO-MSN$_{10}$. Fig. 4(C) shows a TEM image of the GO-MSN$_{10}$ + CPT system, revealing graphene oxide sheets in the micrometric domain decorated with silica nanoparticles (indicated by red arrows); the system retains the structural integrity of the used raw material (GO-MSN$_{10}$) discussed in our previous work.[30] The image also shows needle-shaped

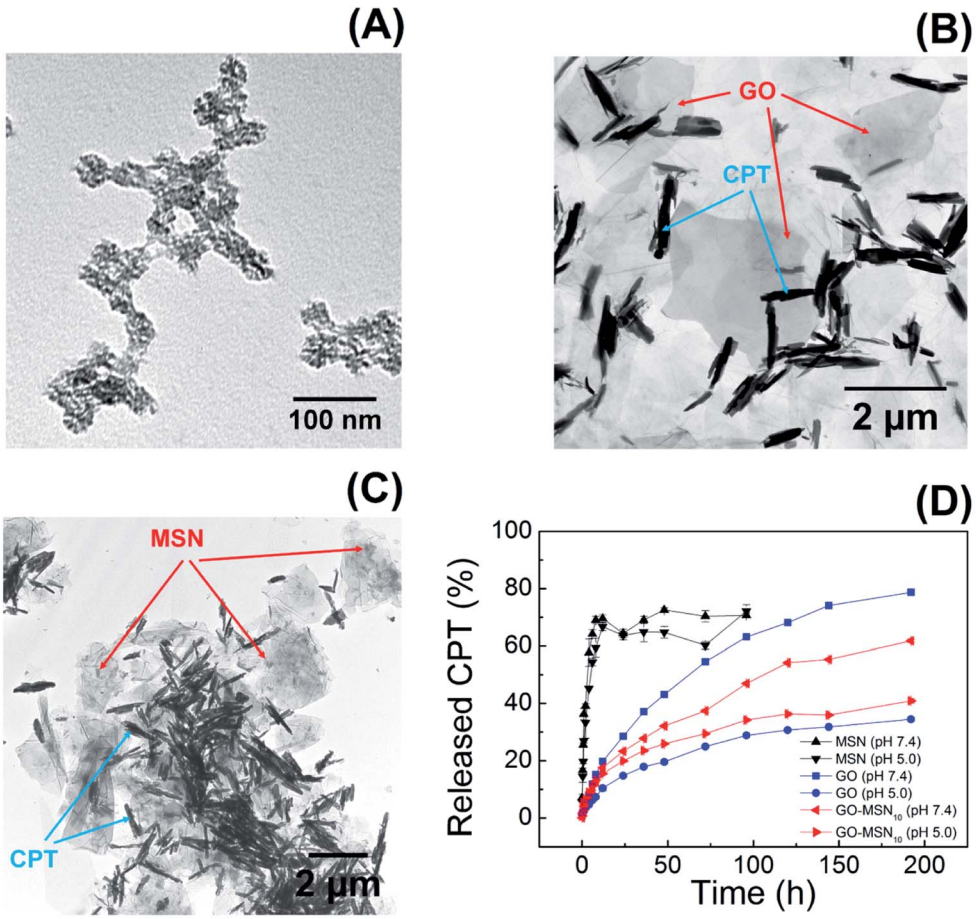

Fig. 4 TEM images of the MSN + CPT (A), GO + CPT (B) and GO-MSN$_{10}$ + CPT (C) systems; camptothecin release graph (D) by MSNs, GO and GO-MSN$_{10}$ at pH 7.4 and 5.0.

camptothecin crystals with similar dimensions to the GO + CPT system and corroborates the mentioned intermolecular association between camptothecin molecules.

The presented set of characterization techniques confirms the preparation of mesoporous silica nanoparticles, graphene oxide and nanocomposite GO-MSN_{10} that contain encapsulated camptothecin. In addition, the UV-Vis, XRD and TEM results collectively suggest the adsorption of camptothecin in the GO and GO-MSN_{10} nanocarriers and show a reduction in π–π restacking after CPT incorporation. As discussed above, a decrease in stacked sheets also occurred after MSN functionalization on the GO surface.

3.2. CPT release studies from the MSN + CPT, GO + CPT and GO-MSN_{10} + CPT materials

Camptothecin release studies were performed for 192 h under sink conditions by using 1% Tween 80 in the release media at pH values of 7.4 (phosphate buffer) and 5.0 (acetate buffer), which mimic, respectively, the pH of fluids under physiological conditions and the cytosol of acid endosomes.

The release graph is shown in Fig. 4(D). The silica nanoparticles show a rapid release of 70% of the encapsulated drug within the first 12 h. In contrast, the graphene oxide and nanocomposite nanomaterials showed a prolonged release profile of up to 78% of the camptothecin over a period of 192 h. First, these results reveal the weak interaction between CPT and MSNs and the strong adsorption of CPT on the surface of the two remaining nanomaterials, corroborating the low encapsulation capacity of silica nanoparticles (8.1 ± 0.4%) and the high antitumor molecule content exhibited by GO + CPT (81.1 ± 3.7%) and GO-MSN_{10} + CPT (80.9 ± 0.9%). In fact, the limited spatial distribution of phenyl groups, restricted by the silica pore structures, can influence the low π–π stacking interactions between CPT and the aromatic groups of this nanocarrier. In the GO and GO-MSN_{10} systems, the sheets have a larger contact area, as characterized by the number of electronically conjugated aromatic rings, which favours more effective π–π interactions in the adsorption of camptothecin. The graph shown in Fig. 4(D) reveals a faster release of camptothecin at pH 7.4 by all nanocarriers. The release from silica is more discrete and almost imperceptible, and the release from graphene oxide and the nanocomposite is significantly more pronounced. Under these conditions, the lactone ring of camptothecin (CPT-lac) is hydrolysed to carboxylate (CPT-$carb^-$),[14–17] which is more hydrophilic species and therefore more soluble in the release medium (hydrophilic), accelerating the release process. Additionally, π–π stacking interactions are attenuated due to lactone ring breaking, which also contributes to the faster release at pH 7.4. The acidification of the environment to pH 5.0 facilitates conversion of the carboxylate function in CPT-$carb^-$ to a lactone ring, generating the more hydrophobic CPT-lac species and favouring higher interactions with the nanomaterials (containing hydrophobic regions) than the external environment (hydrophilic). In this situation, the release rate is slower and prolonged due to the higher drug–nanocarrier interaction. From a biological point of view, camptothecin is inactive during intravenous circulation due to the formation of carboxyl groups by the neutral pH of the blood.[14–17] In the acidic pH environment of the endosomes of cancer cells, the carboxylic group on CPT is converted to a lactone ring, transforming CPT into a biologically active molecule. In this context, a rapid drug release at pH 7.4 by nanocarriers is undesirable because release may occur prior to the nanocarrier reaching the target cell. Therefore, the GO + CPT and GO-MSN_{10} + CPT systems are more promising than silica nanoparticles due to their slow release for 192 h, which is probably sufficient to allow the nanocarriers to reach cells while carrying significant amounts of the drug. From a kinetic point of view, the slow or non-existent delivery of the drug at pH 7 (during systemic circulation) and the faster and more complete release at pH 5.0 (within endosomes) are ideal. Due to the physicochemical characteristics of camptothecin and biological fluids, neutral and acidic conditions show, in all observed situations, faster and slower release rates, respectively; these results are the opposite of ideal conditions. In this context, the optimization of the nanocarriers to reduce the release velocity at pH 7.4 and to accelerate release at pH 5.0 is one of the achieved goals in this work. The comparative analysis of the GO + CPT and GO-MSN_{10} + CPT nanocarriers in the graph in Fig. 4(D) shows the reduction and increase in the delivery rates of camptothecin at pH 7.4 and 5.0, respectively, by the nanocomposite in relation to those with graphene oxide. The results suggest a stronger interaction of camptothecin with the nanocomposite than with graphene oxide at pH = 7 (slower release rate) and weaker interactions of CPT with GO-MSN_{10} than with GO under acidic conditions (faster release rate). In this context, although silica has a fast release profile, its presence on the surface of the graphene oxide is important from the point of view of kinetic modulation of the system and characterizes the difference between the nanocomposite and the GO and MSN nanocarriers. In addition, the GO-MSN_{10} nanomaterial presents significantly reduced haemolysis rates relative to those of graphene oxide, according to our previously published work.[30]

From a physicochemical point of view, the fast release of camptothecin from silica nanoparticles has its origins in the weak interaction of this drug with phenyl groups present inside the pores (see Fig. 5(A)), which explains the low encapsulation capacity of this nanomaterial compared to that of the other nanocarriers. For graphene oxide, the drug–nanocarrier interaction showed significant differences in the release rate under the two studied conditions. At pH 7.4, in which CPT-$carb^-$ is predominant, we propose the following intermolecular interactions: London dispersion interactions between CPT-carb and GO are reduced since the more hydrophilic characteristics of CPT minimize these interactions and increase the solubility of the drug in the environment, enabling dipole–dipole type interactions to prevail. Additionally, negative charges originating from the O^- (hydroxyl) and COO^- (carboxyl) groups on the surface of graphene oxide electrostatically interfere in the repulsion of negative CPT-$carb^-$ molecules, contributing to rapid release. Considering the interior of the dialysis membrane containing GO ↔ (CPT-$carb^-$ = CPT-lac) as the system – where "=" indicates chemical equilibrium and "↔" symbolizes the

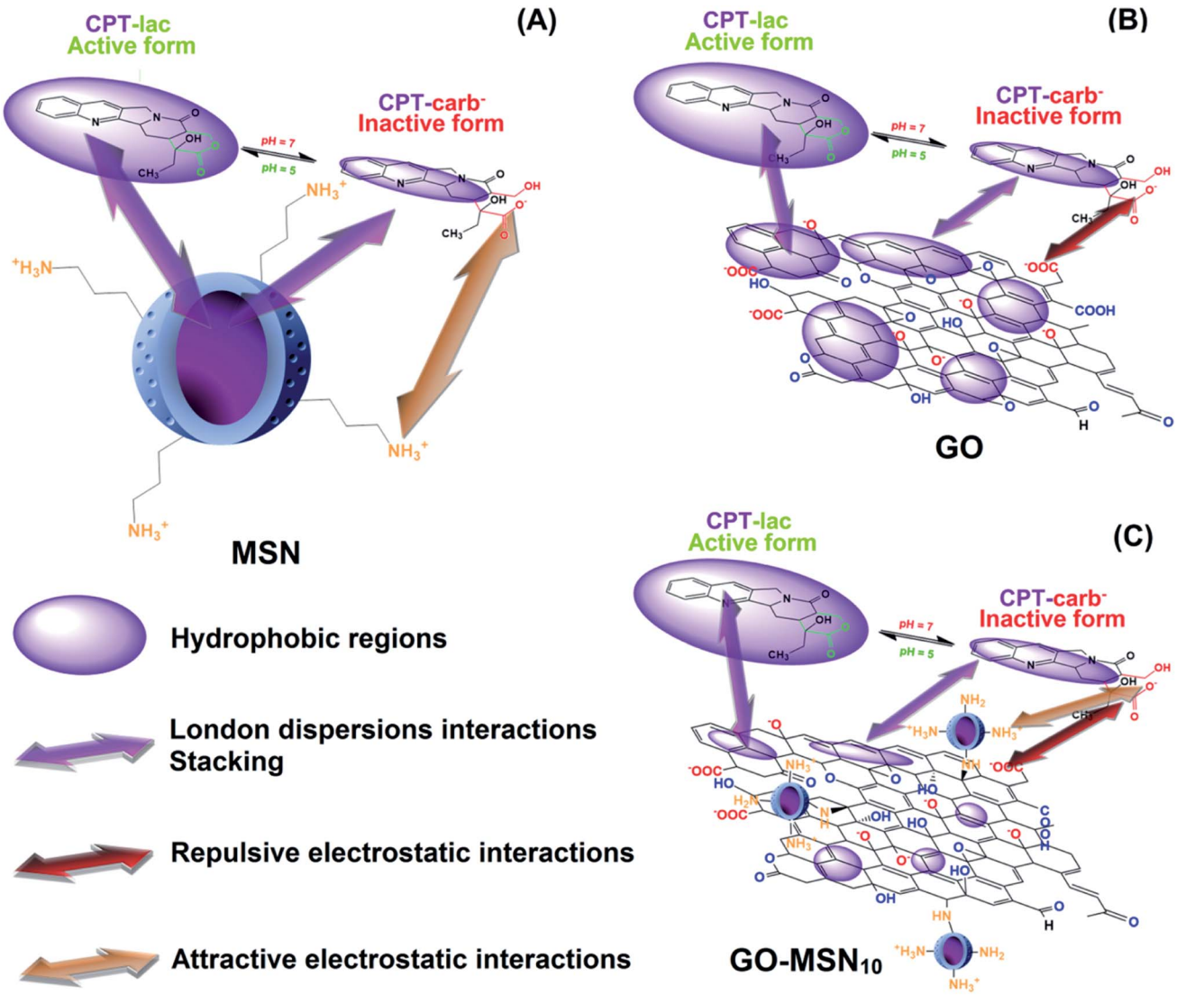

Fig. 5 pH Influence on the chemical equilibrium perturbation between the camptothecin lactone (CPT-lac) and camptothecin carboxylate (CPT-carb$^-$) species in dynamic intermolecular interactions with mesoporous silica nanoparticles (A), graphene oxide (B) and nanocomposite based on graphene oxide decorated with silica nanoparticles (C).

intermolecular interactions between the nanocarrier and the molecule in dynamic chemical equilibrium on its surface – and the release medium as the environment, as CPT-carb$^-$ is eliminated to the environment, the equilibrium moves towards the formation of more CPT-carb$^-$ according to the chemical equilibrium perturbation law of Le Chatelier; the release cycle is repeated, and rapid release to the environment occurs. The functionalization of graphene oxide with silica nanoparticles to form a more hydrophilic nanocomposite (due to the presence of silica with a hydrophilic outer surface) is one of the crucial points explaining the different release rates between GO-MSN$_{10}$ + CPT and GO + CPT. Due to its more hydrophilic character in relation to GO, the nanocomposite presents smaller hydrophobic regions in the sheets of graphene oxide. At pH = 7.4, therefore, the predominant CPT-carb$^-$ species (more hydrophilic) interacts more strongly with the nanocomposite (more hydrophilic than GO), and dipole–dipole type interactions predominate over London dispersion interactions for GO, culminating in a force that contributes to attraction between CPT-carb$^-$ and the nanocomposite in the newly adopted system: GO-MSN$_{10}$ ↔ (CPT-carb$^-$ = CPT-lac). In this situation, there is also competition with the hydrophilic environment. In this context, the dipole–dipole forces act in opposite directions to attract the molecule into the system (towards the nanocarrier) and to release the molecule to the environment (towards the hydrophilic fluid). Interestingly, another attractive force drawing CPT-carb$^-$ towards the surface of GO-MSN$_{10}$ occurs: new electrostatic attractions between the NH_3^+ groups on silica nanoparticles and the negatively charged groups on CPT-carb$^-$ (attractive electrostatic forces are absent in GO and present in GO-MSN$_{10}$). Consequently, the release rate of the most strongly retained antitumor molecule in GO-MSN$_{10}$ at neutral pH is slower than that in GO. Furthermore, the release rate of CPT-carb$^-$ at equilibrium (CPT-carb$^-$ = CPT-lac) is slower in the

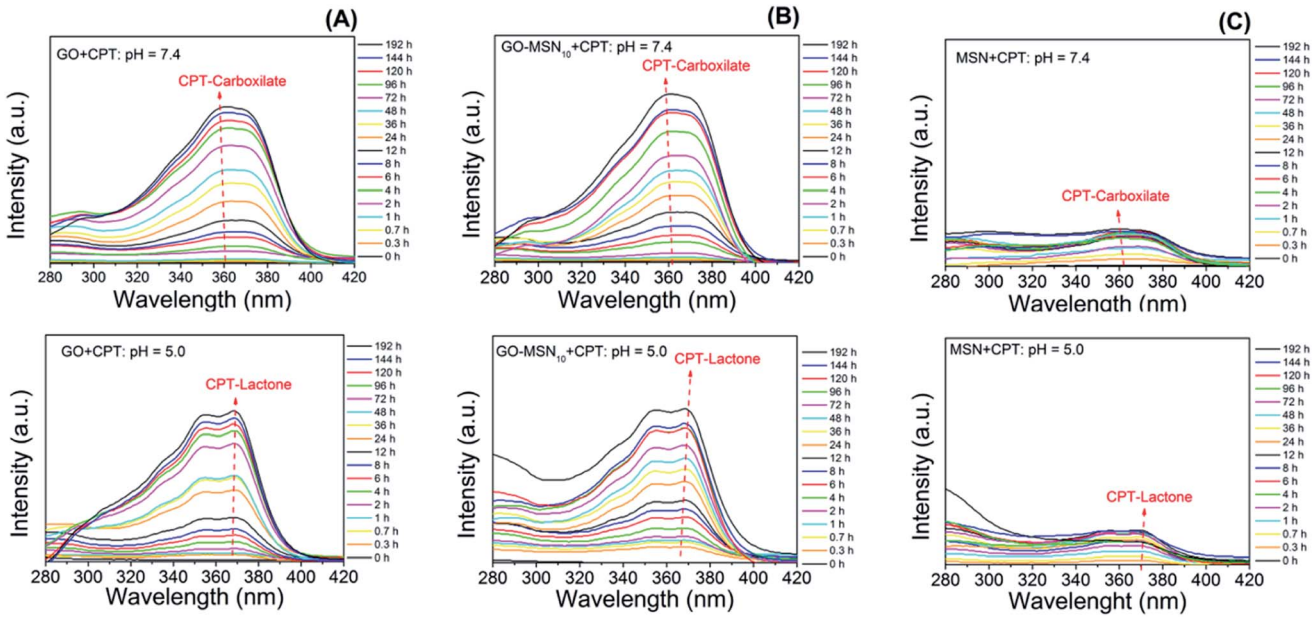

Fig. 6 Influence of pH on the variation of the chemical structure of camptothecin released by graphene oxide (A), nanocomposite (B) and silica (C) nanoparticles.

nanocomposite since fewer camptothecin carboxylate molecules are eliminated to the release medium.

At pH = 5.0, CPT-lac species (hydrophobic) are predominant at chemical equilibrium and begin to interact more strongly with the hydrophobic regions of GO; in this case, London dispersion interactions prevail over dipole–dipole interactions with the hydrophilic external medium. Accordingly, the release of the drug from the system into the environment is significantly slower, and the release rate of CPT-lac from CPT-carb$^-$ to restore equilibrium occurs at significantly reduced velocity. For this reason, the release rates at pH 5.0 are significantly slower than those at pH 7.0 for GO + CPT and GO-MSN$_{10}$ + CPT. This situation is illustrated in Fig. 5(B). In the presence of the acidic release medium, the described chemical equilibrium is shifted towards the formation of the more hydrophobic CPT-lac. In this context, electrostatic forces have no significant influence because the camptothecin lactone ring form is neutral, and in this case, London dispersion forces are more important. As the nanocomposite is more hydrophilic than GO, induced-dipole/induced-dipole interactions (London dispersion) between CPT-lac and GO-MSN$_{10}$ are less pronounced than those between CPT-lac and GO, so CPT interactions with the nanostructure are weaker and release to the external environment is faster at pH 5.0 compared to the results observed for GO + CPT. This phenomenon is illustrated in Fig. 5(C).

To complement the hypothesis regarding the influence of the molecular structure of camptothecin on its UV-Vis spectrum and, consequently, on the observed differences in drug release profiles, a study was carried out to evaluate the molecular structure of CPT in release studies using visible UV-Vis spectroscopy. For this purpose, spectra of the free drug in the release media at pH 5.0 and 7.4 over the course of 192 h were acquired and evaluated. Fig. 6 shows the spectra of camptothecin released at pH 7.4 by GO (Fig. 6(A)), GO-MSN$_{10}$ (Fig. 6(B)) and MSNs (Fig. 6(C)). In these figures, it is notable that the increase in the absorbance of a broad band at approximately 365 nm, corresponding to the n → π* electronic transitions of camptothecin, is proportional to the concentration of this molecule. In the spectra of CPT released from the nanomaterials at pH 5.0 (Fig. 6(A–C)), two shoulders at approximately 355 and 370 nm are clearly visible in the GO + CPT, GO-MSN$_{10}$ + CPT and MSN + CPT spectra at all release times, which are also related to n → π* electronic transitions. These observed shoulders correspond to electronic transitions occurring in the antitumor molecule with the lactone organic function (mostly formed at pH = 5.0). After hydrolysis of this function to generate the carboxylate species in pH = 7.4, the said shoulders are not observed, and as a result, the broad band at 365 nm is typical of the CPT-carb$^-$ molecular structure. Thus, the present study corroborates the discussions regarding CPT release experiments and is in agreement with the data in the literature.[34]

The above discussion clearly shows the differences in the nanocomposite based on graphene oxide decorated with silica nanoparticles as a nanocarrier; this material has optimized drug delivery characteristics compared with those of MSN and GO materials. These properties suggest the potential application of GO-MSN nanomaterials as nanocarriers in antitumor treatment.

4. Conclusion

Characterization techniques comprising UV-Vis, XRD and TEM confirm the encapsulation of camptothecin in three types of nanomaterials: mesoporous silica nanoparticles (MSNs), graphene oxide (GO) and a nanocomposite based on graphene oxide decorated with silica nanoparticles (GO-MSN$_{10}$). An

unexpected phenomenon of CPT–CPT association on the surface of GO and GO-MSN_{10} was proposed and discussed in terms of intermolecular forces, including hydrogen bonds and π–π stacking interactions. Drug release studies in conjunction with the characterization results showed a rapid camptothecin release by silica nanoparticles (12 h) and prolonged release by the GO and GO-MSN_{10} materials (192 h). The antitumor molecule has a higher chemical interaction with the latter two materials, and the presence of silica nanoparticles on the surface of the graphene oxide showed strategic importance in the modulation and optimization of the release rate at pH 7.4 (relevant to the physiological conditions in living organisms) and pH 5.0 (relevant to the endosomes of cancer cells), indicating that the GO-MSN_{10} nanomaterial is a potential candidate for antitumor applications with lower risk in the context of nanosafety.

Conflicts of interest

There are no conflicts to declare.

Acknowledgements

The authors would like to acknowledge the financial support from CAPES, INCT-Inomat, Brazilian Nanotoxicology Network (Cigenanotox) and NanoBioss/MCTIC.

References

1 K. D. Miller, R. L. Siegel, C. C. Lin, A. B. Mariotto, J. L. Kramer, J. H. Rowland, K. D. Stein, R. Alteri and A. Jemal, *CA A Cancer J. Clin.*, 2016, **66**, 271–289.
2 R. L. Siegel, K. D. Miller and A. Jemal, *CA A Cancer J. Clin.*, 2017, **67**, 7–30.
3 L. Fan, Y. Zhang, F. Wang, Q. Yang, J. Tan, R. Grifantini, H. Wu, C. Song and B. Jin, *Biomaterials*, 2016, **76**, 399–407.
4 Q. Hu, W. Sun, C. Wang and Z. Gu, *Adv. Drug Delivery Rev.*, 2016, **98**, 19–34.
5 X. Zhang, J. Ge, Y. Xue, B. Lei, D. Yan, N. Li, Z. Liu, Y. Du and R. Cai, *Chem.–Eur. J.*, 2015, **21**, 11954–11960.
6 T. M. Allen and P. R. Cullis, *Science*, 2004, **303**, 1818.
7 L. C. Fonseca, A. J. de Paula, D. S. T. Martinez and O. L. Alves, *New J. Chem.*, 2016, **40**, 8060–8067.
8 L. Qing-Yong, Z. Yuan-Gang, S. Rong-Zhen and Y. Li-Ping, *Curr. Med. Chem.*, 2006, **13**, 2021–2039.
9 M. Jedrzejczak-Silicka, K. Urbas, E. Mijowska and R. Rakoczy, *J. Alloys Compd.*, 2017, **709**, 112–124.
10 L. F. Liu, S. D. Desai, T.-K. Li, Y. Mao, M. E. I. Sun and S.-P. Sim, *Ann. N. Y. Acad. Sci.*, 2000, **922**, 1–10.
11 V. J. Venditto and E. E. Simanek, *Mol. Pharmaceutics*, 2010, **7**, 307–349.
12 S. Yu, Q.-Q. Huang, Y. Luo and W. Lu, *J. Org. Chem.*, 2012, **77**, 713–717.
13 Z. Blanka, W. Tomasz, C. Michal and K. Stefan, *Comb. Chem. High Throughput Screen.*, 2016, **19**, 319–324.
14 J. Cheng, K. T. Khin and M. E. Davis, *Mol. Pharmaceutics*, 2004, **1**, 183–193.
15 Y. Çirpanli, E. Bilensoy, A. Lale Doğan and S. Çaliş, *Eur. J. Pharm. Biopharm.*, 2009, **73**, 82–89.
16 M. Ma, P. Xing, S. Xu, S. Li, X. Chu and A. Hao, *RSC Adv.*, 2014, **4**, 42372–42375.
17 N. K. Thakral, A. R. Ray, D. Bar-Shalom, A. H. Eriksson and D. K. Majumdar, *AAPS PharmSciTech*, 2012, **13**, 59–66.
18 P. Gong, Q. Zhao, D. Dai, S. Zhang, Z. Tian, L. Sun, J. Ren and Z. Liu, *Chem.–Eur. J.*, 2017, **23**, 17531–17541.
19 K. Peng and H. Yang, *Chem. Commun.*, 2017, **53**, 6085–6088.
20 B. Shi, X. Du, J. Chen, L. Fu, M. Morsch, A. Lee, Y. Liu, N. Cole and R. Chung, *Small*, 2017, **13**, 1603966.
21 P. Song, S. Kuang, N. Panwar, G. Yang, D. J. H. Tng, S. C. Tjin, W. J. Ng, M. B. A. Majid, G. Zhu, K.-T. Yong and Z. L. Wang, *Adv. Mater.*, 2017, **29**, 1605668.
22 T. Kavitha, I.-K. Kang and S.-Y. Park, *Colloids Surf., B*, 2014, **115**, 37–45.
23 C. Shan, H. Yang, D. Han, Q. Zhang, A. Ivaska and L. Niu, *Langmuir*, 2009, **25**, 12030–12033.
24 X. Yang, N. Zhao and F.-J. Xu, *Nanoscale*, 2014, **6**, 6141–6150.
25 Z.-Y. Li, Y. Liu, X.-Q. Wang, L.-H. Liu, J.-J. Hu, G.-F. Luo, W.-H. Chen, L. Rong and X.-Z. Zhang, *ACS Appl. Mater. Interfaces*, 2013, **5**, 7995–8001.
26 M. Ma, H. Xu, H. Chen, X. Jia, K. Zhang, Q. Wang, S. Zheng, R. Wu, M. Yao, X. Cai, F. Li and J. Shi, *Adv. Mater.*, 2014, **26**, 7378–7385.
27 A. J. Paula, R. T. Araujo Júnior, D. S. T. Martinez, E. J. Paredes-Gamero, H. B. Nader, N. Durán, G. Z. Justo and O. L. Alves, *ACS Appl. Mater. Interfaces*, 2013, **5**, 8387–8393.
28 A. Arshad, J. Iqbal, Q. Mansoor and I. Ahmed, *J. Appl. Phys.*, 2017, **121**, 244901.
29 Z. Zhang, J. Shi, Z. Song, X. Zhu, Y. Zhu and S. Cao, *J. Mater. Sci.*, 2018, **53**, 1810–1823.
30 L. C. Fonseca, M. M. de Araújo, A. C. M. de Moraes, D. S. da Silva, A. G. Ferreira, L. S. Franqui, D. S. T. Martinez and O. L. Alves, *Appl. Surf. Sci.*, 2018, **437**, 110–121.
31 H. Huang, J. Zhang, L. Jiang and Z. Zang, *J. Alloys Compd.*, 2017, **718**, 112–115.
32 L. Zhang, W. Wang, J. Cheng, Y. Shi, Q. Zhang, P. Dou and X. Xu, *J. Mater. Sci.*, 2018, **53**, 787–798.
33 H.-F. Cui, W.-W. Wu, M.-M. Li, X. Song, Y. Lv and T.-T. Zhang, *Biosens. Bioelectron.*, 2018, **99**, 223–229.
34 M. de Sousa, L. A. V. de Luna, L. Fonseca, S. Giorgio and O. L. Alves, *ACS Appl. Nano Mater.*, 2018, **1**, 922–932.
35 J.-M. Shen, F.-Y. Gao, L.-P. Guan, W. Su, Y.-J. Yang, Q.-R. Li and Z.-C. Jin, *RSC Adv.*, 2014, **4**, 18473–18484.
36 K.-H. Liao, Y.-S. Lin, C. W. Macosko and C. L. Haynes, *ACS Appl. Mater. Interfaces*, 2011, **3**, 2607–2615.
37 S. Sahu, N. Sinha, S. K. Bhutia, M. Majhi and S. Mohapatra, *J. Mater. Chem. B*, 2014, **2**, 3799–3808.
38 Z. Xu, S. Liu, Y. Kang and M. Wang, *Nanoscale*, 2015, **7**, 5859–5868.
39 Y. Yan, J. Fu, T. Wang and X. Lu, *Acta Biomater.*, 2017, **51**, 471–478.
40 L. Huang, Y. Zhang, H. Liu, B. Liu and M. Tu, *New J. Chem.*, 2014, **38**, 5817–5824.

41 Y. Yang, Y. Liu, C. Cheng, H. Shi, H. Yang, H. Yuan and C. Ni, *ACS Appl. Mater. Interfaces*, 2017, **9**, 28195–28208.
42 J. Dey and I. M. Warner, *J. Lumin.*, 1997, **71**, 105–114.
43 J. Li, C.-y. Liu and Y. Liu, *J. Mater. Chem.*, 2012, **22**, 8426–8430.
44 H. Bao, Y. Pan, Y. Ping, N. G. Sahoo, T. Wu, L. Li, J. Li and L. H. Gan, *Small*, 2011, **7**, 1569–1578.
45 T. Kavitha, S. I. Haider Abdi and S.-Y. Park, *Phys. Chem. Chem. Phys.*, 2013, **15**, 5176–5185.
46 D. Dvoranová, M. Bobeničová, S. Šoralová and M. Breza, *Chem. Phys. Lett.*, 2013, **580**, 141–144.
47 Y. Harada, T. Yamamoto, M. Sakai, T. Saiki, K. Kawano, Y. Maitani and M. Yokoyama, *Int. J. Pharm.*, 2011, **404**, 271–280.
48 Q. Pei, X. Hu, Z. Li, Z. Xie and X. Jing, *RSC Adv.*, 2015, **5**, 81499–81501.

